Oct 19th, 12:00 AM

Fire Resistance of Loadbearing LSF Assemblies

Farid Alfawakhiri

Mohamed A. Sultan

Fifteenth International Specialty Conference on Cold-Formed Steel Structures
St. Louis, Missouri U.S.A., October 19-20, 2000

FIRE RESISTANCE OF LOADBEARING LSF ASSEMBLIES

By Farid Alfawakhiri[1] and Mohamed A. Sultan[2]

ABSTRACT

This paper presents an analytical thermal-structural model for loadbearing lightweight steel framed (LSF) walls exposed to fire on one side. The model reflects temperature and deformation data from six standard fire resistance tests conducted recently by the National Research Council of Canada in partnership with the North American steel industry. Some characteristic patterns in thermal transmission and structural behaviour are discussed. Temperature histories across LSF assemblies are simulated numerically by explicit integration of transient heat transfer equations. The apparent thermal properties are calibrated for gypsum board and three types of insulation. Analytical procedures are presented to simulate lateral deformation histories and predict structural failure times. The model illustrates how different heating regimes in cold formed steel studs cause different structural failure modes.

INTRODUCTION

Lightweight steel framed (LSF) assemblies are required in many instances (NBCC 1995) to provide adequate fire resistance in order to prevent or delay the spread of fire and ensure that building integrity is maintained during fires, while occupants evacuate and fire fighters perform suppression and rescue operations. Existing North American codes require the fire resistance ratings of structural assemblies to be determined on the basis of standard fire resistance tests, according to CAN/ULC-S101-M89 or ASTM E119-95a, which are quite expensive and time consuming. The number of LSF assemblies tested for fire resistance is limited compared to the variety of designs that LSF technology can offer. The ongoing evolution of performance-based codes provides a stimulus for the development of new, analytical, methods of establishing the fire resistance of LSF assemblies. Reliable numerical models, based on fundamental principles of chemistry, physics and engineering of structural fire protection, are becoming the essential tools to achieve cost-effective designs while maintaining high levels of fire safety. Computational techniques are especially needed where non-standard fire exposures must be considered.

A survey of relevant literature has been presented elsewhere (Alfawakhiri et al. 1999). Here, an analytical fire resistance model for loadbearing LSF walls is presented, based on recent experimental data from six standard fire resistance tests.

[1] Research Fellow, Canadian Steel Construction Council, Toronto, Canada
[2] Senior Research Officer, Fire Risk Management Program, Institute for Research in Construction, National Research Council of Canada, Ottawa, Canada

FIRE RESISTANCE TESTS

The wall assemblies tested (designated W1 through W6) were 3048 mm high by 3658 mm long. Each assembly consisted of a single row of galvanized cold-formed steel studs, protected with two layers of 12.7-mm thick fire-resistant gypsum board (Type X Firecode C) on each side. All steel studs had a C-shaped cross-section, nominally, 92.1 mm deep by 41.3 mm wide, with 12.5-mm flange stiffening lips and base metal thickness of 0.912 mm (control measurements showed an average thickness under-run of 0.01 mm). The minimum specified steel yield strength was F_y = 228 MPa. Each stud had four web perforations, 38 mm wide, spaced 610 mm o.c. along the stud. Figure 1 illustrates a typical steel frame fabrication layout for wall specimens. Table 1 lists the variable parameters for the tests. The purpose of this test series was to investigate the effects of stud spacing, resilient channels and insulation type on the fire resistance of loadbearing LSF walls.

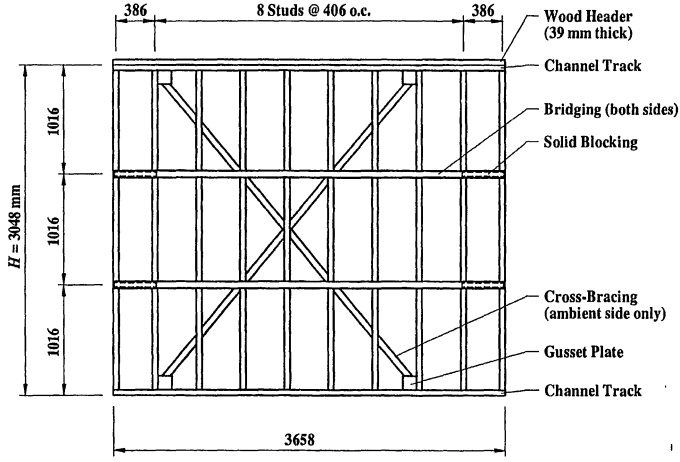

Figure 1. Typical steel frame fabrication layout for wall specimens.

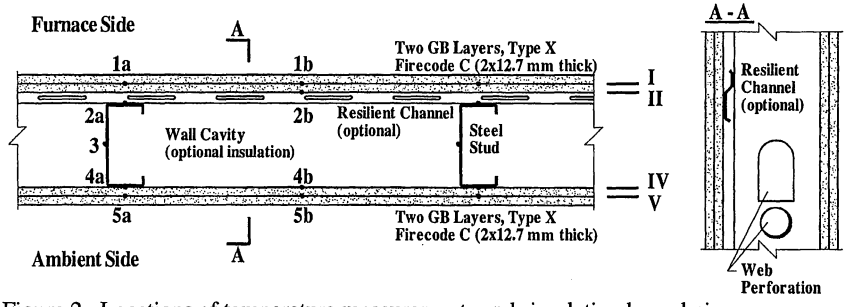

Figure 2. Locations of temperature measurements and simulation boundaries.

Table 1. Summary of fire resistance tests on loadbearing LSF walls.

Specimen number	Stud spacing (mm)	Insulation type (fibre)	Resilient channels on exposed side	Load including self-weight (kN/m)	Fall-off time of gypsum board on exposed side (min)		Structural failure time (min)	Temperature rise on unexposed side, under pads, at failure time (°C)	
					Face layer	Base layer		Maximum	Average
W1	406	Glass	Yes	21.5	50	in place	55	52	36
W2	610	Rock	Yes	14.3	57	67	73	50	42
W3	406	Cellulose	Yes	21.5	57	in place	70	42	37
W4	406	-	Yes	21.5	58	in place	76	64	60
W5	406	Rock	Yes	21.5	53	in place	59	37	26
W6	406	-	No	21.5	in place	in place	83	76	69

Various types of insulation and resilient channels are often used in LSF wall designs to improve their sound transmission classification (STC) ratings. Three types of insulation were used in the tests: glass fibre batts, rock fibre batts and dry blown cellulose. Nine resilient channels, attached perpendicular to studs and spaced 406 mm o.c., were used in each test, except W6, to support the gypsum board on the fire-exposed side. The resilient channels, 14 mm deep and 58 mm wide, were fabricated from 0.6-mm thick galvanized steel sheets. Figure 2 schematically illustrates the cross-sectional details of the wall specimens. An exhaustive description of wall construction details and the test setup is presented elsewhere (Kodur et al. 1999).

The wall specimens were loaded vertically between two parallel rigid beams and subjected to standard fire on one side. In accordance with CAN/ULC-S101-M89 requirements, nine thermocouples were placed under standard pads on the unexposed side of the wall in each test. These thermocouples were meant to detect the heat penetration failure (if any) of the specimens, according to the standard criteria: a single point temperature rise of 180°C, or an average temperature rise of 140°C, above the ambient temperature. In addition, at least 50 thermocouples were placed in each specimen at various locations in order to generate experimental data for heat transfer analytical studies. These additional thermocouples were arranged in two groups, symmetric about a horizontal plane at the mid-height of the wall, at two elevation levels: 762 mm from the bottom of the wall (0.25 H level, where H = wall height =3048 mm) and 2286 mm from the bottom of the wall (0.75 H level). The generalized locations of thermocouples are shown in Figure 2 designated by Arabic figures. Most of the thermocouples were distributed within the central part of wall specimens, about 2 m long. In several tests, temperature measurements were also conducted at wall ends. Horizontal (lateral) deflections of wall specimens were measured by potentiometers, on the unexposed side, at nine locations in each test. These measurements were conducted at three elevation levels (0.25 H, 0.5 H and 0.75 H levels) at three studs in the central part of each wall specimen.

A short summary of test results is provided in Table 1. The listed structural failure times represent the number of full minutes passed since the ignition of the furnace before the loss of specimen's ability to sustain the applied load. Gypsum board fall-off times, shown in the table, indicate the number of full minutes passed since the ignition of the furnace before the fall-off of a layer piece not less than 500 mm in any dimension. Figure 3 shows histories of average temperatures, designated by respective generalized location numbers, measured in the central part of wall specimens. Plots of average lateral deflections are presented in Figure 4. Positive deflections indicate movement towards the furnace. Large lateral deflections were recorded at all elevation levels at the end of all tests, as structural failure resulted in the overall out-of-plane buckling of the walls. These large deflections are not shown on the figure in order to maintain an appropriate scale of the plots.

The following trends in the behaviour of loadbearing LSF walls, exposed to standard fire, have been established based on experimental observations and measured data:

- Heat penetration failure was not detected in any of the tests. All specimens failed by losing their ability to sustain the applied load (i.e., exhibited structural failure). As shown in Table 1, the temperature rise on the unexposed side was considerably (at least 70°C) below standard failure criteria by the end of the tests. This suggests that much higher fire resistance ratings are likely to be achieved in fire tests on similar non-loadbearing LSF walls. Clearly, loading significantly reduces fire resistance.
- In all tests, two layers of 12.7-mm thick fire-resistant gypsum board provided about 40 minutes of delay in the temperature rise in the hot flanges of the studs (generalized location 2a). The duration of this delay can be regarded as a stable property of the gypsum board used in tests, as it seems to be insensitive to the variable parameters of this test series.
- Comparison of Tests W1, W3 and W5 versus Test W4 suggests that insulation placed in wall cavity reduces the fire resistance of loadbearing LSF walls.
- Insulation restricts the passage (and dissipation) of heat through the cavity causing an accelerated temperature rise in the hot flanges, and a delayed temperature rise in the cold flanges, of the studs. Therefore, the heating regime of studs in insulated walls features high temperature gradients across the steel section, while the heating regime of studs in non-insulated walls is rather close to uniform heating. The development of lateral deflections (thermal bowing) correlates well with the development of temperature gradients across the steel section.
- Structural failure resulted in overall buckling towards the furnace for non-insulated walls (W4 and W6) and away from furnace for insulated walls (W1-W3 and W5). The dominant failure mode for studs in non-insulated walls was the compressive failure of the cold flange near mid-height, as illustrated in Fig. 5a. The dominant failure mode for studs in insulated walls was the compressive failure of the hot flange at the location of the first web perforation (0.2 H level), as shown in Fig. 5b. This difference in the observed structural behaviour of steel studs in non-insulated and insulated walls can be attributed to the difference in the heating regimes described above.
- The positive peaks in the 0.25 H lateral deflection curves, for insulated walls, of Figure 4 indicate the beginning of stud movement away from the furnace. They reflect the initiation of the failure mechanism in the central studs of insulated walls.

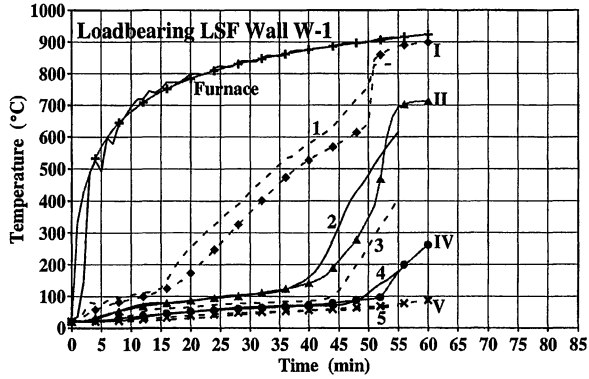

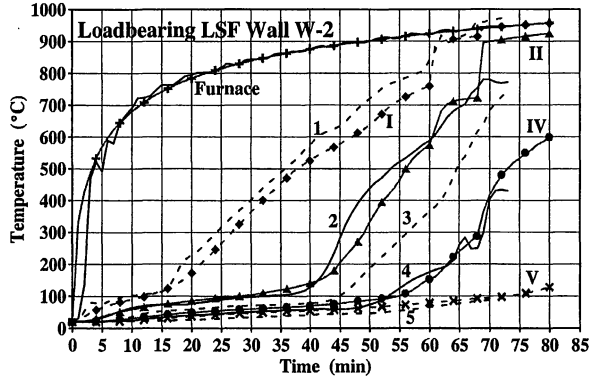

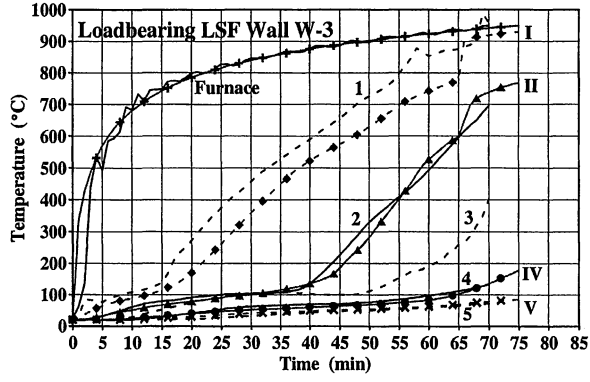

Figure 3. Measured and simulated temperature histories.

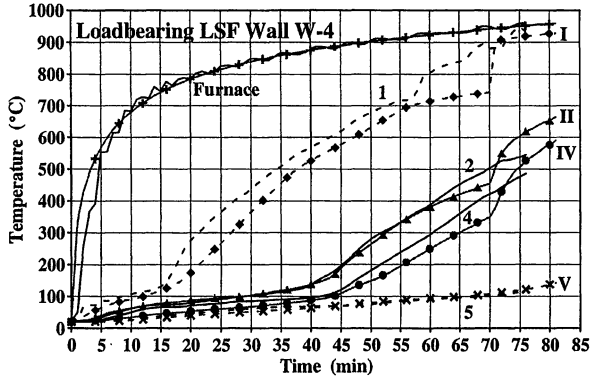

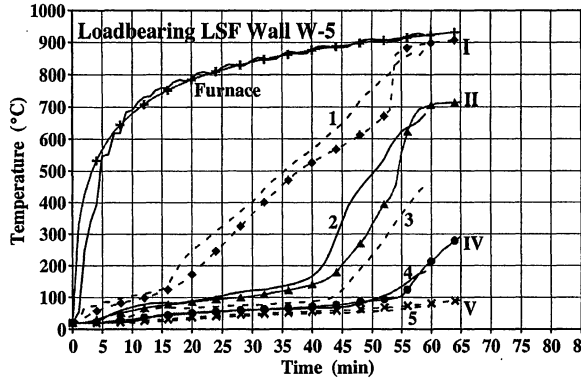

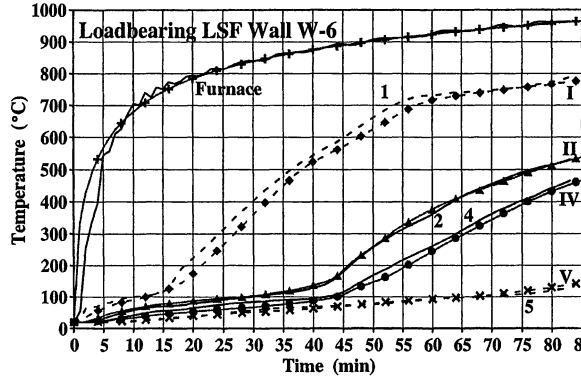

Figure 3 (continued). Measured and simulated temperature histories.

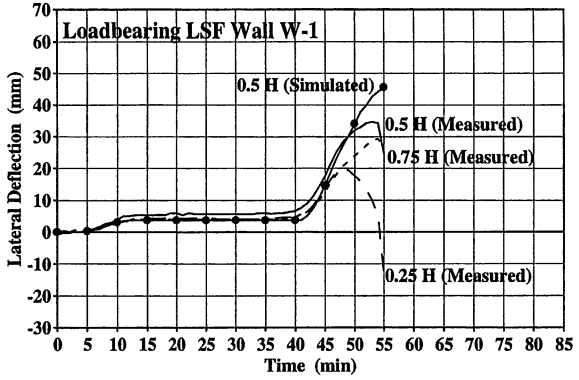

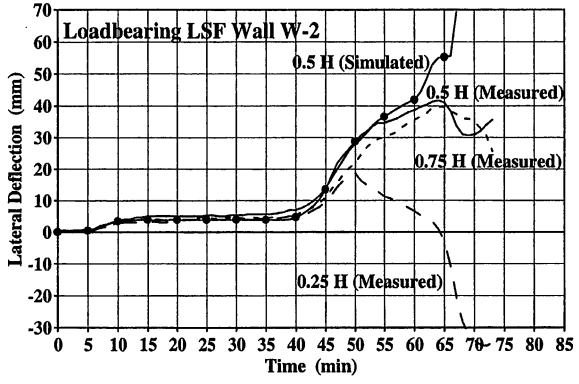

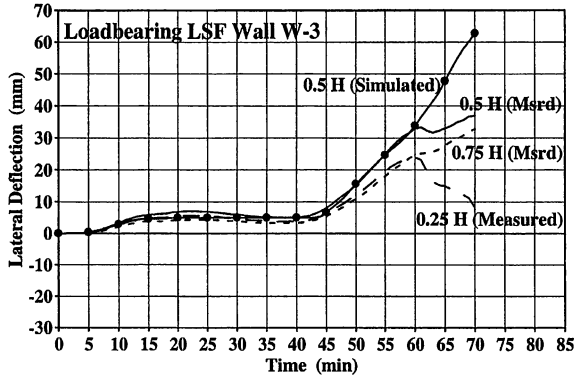

Figure 4. Measured and simulated histories of lateral deflection.

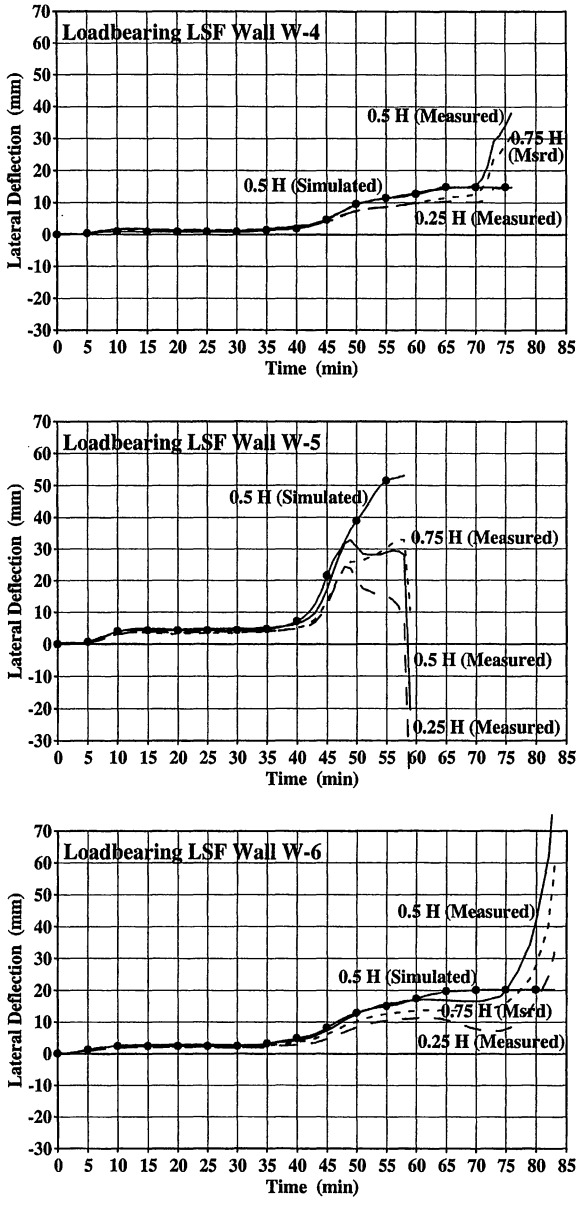

Figure 4 (continued). Measured and simulated histories of lateral deflection.

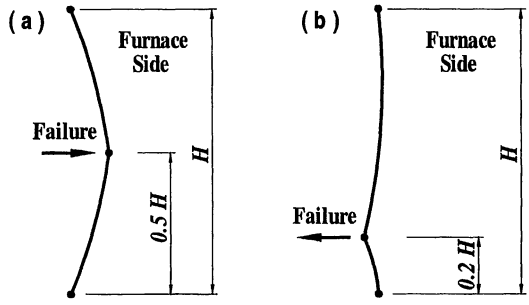

Figure 5. Structural failure modes: (a) non-insulated walls, (b) insulated walls.

• The temperature rise at wall ends proceeded significantly slower than in the central part of specimens, especially during tests on insulated walls. Figure 6 illustrates this trend, as it shows the average hot flange and cold flange temperatures measured at the end studs of wall W2 compared to respective average temperatures in the central part of the specimen. As a result, the end studs were subjected to smaller temperature gradients and exhibited smaller thermal bowing than the remaining studs in the central part of specimens. The structural failure modes of the end studs were usually different from the dominant failure modes of the central studs.

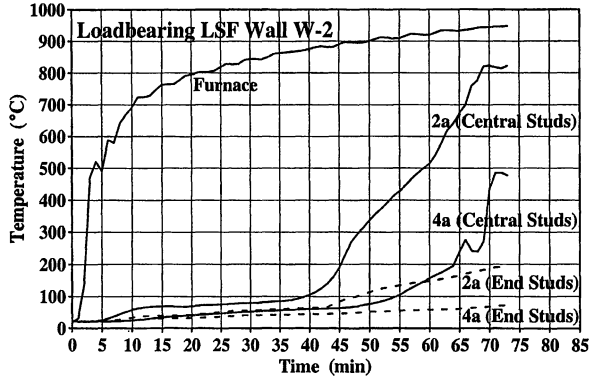

Figure 6. Comparison of average temperatures measured at central and end studs.

• Comparison of Test W2 versus Test W5 indicates that wider stud spacing is beneficial for the fire resistance of loadbearing LSF walls in standard tests. For a given service load per stud, wider stud spacing results in smaller total test load (due to fewer studs in the assembly). Since the wall specimens are loaded between rigid beams, the two

colder studs at wall ends are largely responsible for resisting this total load during the final phase of the fire test. Therefore, a reduction in total load significantly improved fire resistance in Test W2. Contrary to a generally held belief, wider stud spacing of loadbearing LSF walls should not be associated with a reduction in their fire resistance.

- Comparison of Test W4 versus Test W6 suggests that resilient channels reduce the fire resistance of LSF walls, because they reduce the ability of the fire exposed gypsum board to stay in place.

NUMERICAL MODELLING

Heat Transfer Simulations

Retrospective numerical simulations of temperature histories were conducted using the computer program TRACE (Temperature Rise Across Construction Elements), which employs an explicit integration algorithm (Sultan 1996) to solve one-dimensional transient heat transfer equations. The presence of the steel frame was neglected in these thermal simulations, because, due to it's light weight, it plays a minor role in the heat transfer mechanism. Temperature histories were generated at the boundaries shown in Figure 2 designated by Roman figures. The simulated histories, designated by respective boundary numbers, are presented in Figure 3 (curves with symbols). The thermal properties of wall materials used in these simulations are summarized in Tables 2 and 3.

A large number of numerical trial runs have been conducted to achieve a reasonable agreement of simulated and measured temperature histories at all four boundaries in all

Table 2. Apparent thermal properties of Type X Firecode C gypsum board (bulk density 750 kg/m^3).

Apparent thermal properties	Temperature range (°C)											
	<50	50--80	80--100	100--120	120--140	140--160	160--180	180--200	200--300	300--500	500--700	>700
Conductivity [W/(m°C)]	0.27	0.27	0.27	0.15	0.15	0.15	0.15	0.15	0.17	0.17	0.25	0.45
Heat capacity [MJ/(m^3°C)]	0.49	0.70	1.4	2.8	5.6	9.1	7.0	2.8	2.8	1.4	0.49	0.35

Table 3. Apparent thermal properties of insulation materials.

Insulation type (bulk density in kg/m^3)	Apparent heat capacity [MJ/(m^3°C)]	Apparent thermal conductivity [W/(m°C)] in temperature range (°C)						
		<80	80--200	200--300	300--400	400--500	500--700	>700
Rock fibre batts (33 kg/m^3)	0.027	1.0	0.50	0.10	0.10	1.5	2.0	3.0
Glass fibre batts (10 kg/m^3)	0.009	1.0	0.50	0.10	0.10	1.5	2.0	3.0
Loose fill cellulose (47 kg/m^3)	0.115	1.0	0.3	0.30	0.30	1.0	1.0	2.0

six tests. Material properties, thermal conductivity and heat capacity at temperatures up to 1000°C, were found to have a great deal of influence on the shape of simulated time-temperature curves. The properties listed in Tables 2 and 3 were essentially calibrated to produce a good match of numerical and test results. These apparent thermal properties implicitly account for physical phenomena other than heat transfer, such as mass transfer, phase change, etc.

Another parameter to have a major effect on temperature histories is the fall-off time of gypsum board layers. TRACE models the spalling of gypsum board by removing it from the simulation at user-specified time. The fall-off times listed in Table 1 reflect the beginning of layer spalling based on visual test observations. In the simulations of Figure 3, these times were adjusted (increased) for Tests W2-W5 in order to represent a time when a significant portion of the layer had fallen off. Sensitivity analysis was conducted for all other numerical parameters, and it should be mentioned that temperature histories are not very sensitive to emissivity or convection coefficients.

Structural Model

The structural behaviour of an LSF wall, exposed to fire on one side, is modelled here by a single stud with initial imperfection subjected to eccentric tributary load, P, as shown in Figure 7. The following assumptions are employed:

- Steel stress-strain relationships at elevated temperatures are linear up to the yield strength.
- Flexural-torsional and weak axis buckling failure modes are prevented by adequate lateral restraints.
- The stud is hinged at the ends.
- There is no temperature variation in the vertical direction along the stud; however, the temperature varies across the stud section from T_H at the hot flange to T_C at the cold flange.

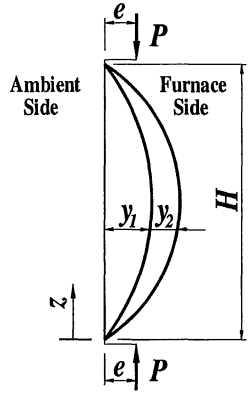

Figure 7. Thermal bowing and secondary deflection.

Further, assuming a linear gradient of thermal elongation strain across the stud section, the thermal bowing curvature, φ , can be expressed by

$$\varphi = \alpha_T \, \delta_T / D \qquad [1]$$

where thermal expansion coefficient α_T for steel (Lie 1992)

$$\alpha_T = (12+0.004 \, T_A) \cdot 10^{-6} \qquad [2]$$

and
D = stud section depth,
$\delta_T = T_H - T_C$ = temperature difference across stud section in °C,
$T_A = 0.5 \, (T_H + T_C)$ = average stud temperature in °C.

Then, the shape of the stress-free initial imperfection, $y_1(z)$, caused by thermal bowing, is

$$y_1(z) = 0.5 \, \varphi \, z \, (H - z) \qquad [3]$$

The vertical load, P, acting with an eccentricity, e, causes secondary lateral deflection, $y_2(z)$, as shown in Figure 7. The differential equation for the system

$$- E \, I^* \, y_2''(z) = P \, [\, y_1(z) + y_2(z) - e \,] \qquad [4]$$

can be solved for the total lateral deflection

$$y(z) = y_1(z) + y_2(z) = \, (\varphi \, \beta^{-2} - e) \, [\tan(0.5 \beta H) \sin(\beta z) + \cos(\beta z) - 1] \qquad [5]$$

where $\beta^2 = P / (E \, I^*)$ [6]

I^* = elasticity-modulus-weighted moment of inertia of the unreduced stud section about the neutral axis parallel to flanges, and
E = 203000 MPa = steel modulus of elasticity at room temperature.

This model adopts the following expression (Gerlich et al. 1996) to account for the reduction in steel modulus of elasticity at elevated temperatures

$$n_T = E_T / E = 1.0 - 3.0 \cdot 10^{-4} \, T + 3.7 \cdot 10^{-7} \, T^2 - 6.1 \cdot 10^{-9} \, T^3 + 5.4 \cdot 10^{-12} \, T^4 \qquad [7]$$

where E_T = modulus of elasticity of steel at temperature T (in °C).

Due to temperature variation from hot flange to cold flange, the modulus of elasticity varies across the steel stud section, and the 'modulus-weighted' moment of inertia in Eq.6 accounts for this variation. I^* can be quantified numerically by dividing the stud section into a sufficiently large number, q , of two-dimensional elements, so that

$$I^* = \sum_{i=1}^{q} n_i \, [I_i + A_i (x_i - c)^2] \qquad [8]$$

where
n_i = reduction factor for temperature T_i, calculated using Eq.7,
I_i = moment of inertia of element i about its own neutral axis parallel to flanges,
A_i = area of element i,
x_i = distance of element i from the extreme fibre of the cold flange,
T_i = temperature of element i, calculated from

$$T_i = T_C + (\delta_T \, x_i / D) \qquad [9]$$

and
c = distance from the centroidal axis of the 'modulus-weighted' section to the extreme fibre of the cold flange, calculated from

$$c = \sum_{i=1}^{q} n_i \, A_i \, x_i \Big/ \sum_{i=1}^{q} n_i \, A_i \qquad [10]$$

The eccentricity, e, appears in the model for the following reasons:

- As the temperature gradient develops across the stud, and the modulus of elasticity deteriorates at the hot flange, the centre of the steel section shifts towards the cold flange.
- The test loading conditions for LSF walls were close to loading between two parallel plates. Therefore, rotation of stud ends, associated with thermal bowing, causes the shift of the load towards the hot flange.
- The assumed stress-free thermal bowing is an idealization of the real stress condition caused by heating. Eccentricity in part simulates internal stresses caused by non-linear thermal strain gradients.

Clearly, eccentricity strongly depends on δ_T, and it is convenient to assume e proportional to $\varphi \, \beta^{-2}$

$$e = (1 - K_R) \, \varphi \, \beta^{-2} \qquad [11]$$

where K_R is a reduction coefficient.

Substitution of Eq.11 into Eq.5 for z=0.5H gives the expression for the lateral deflection, Δ, at the mid-height of the stud

$$\Delta = K_R \, \varphi \, \beta^{-2} \; [\, 1 / \cos(0.5 \beta H) - 1 \,] \qquad [12]$$

Equations 1 to 12 were incorporated into computer program STUD that has been developed to model the structural behaviour of loadbearing LSF walls in fire resistance tests. In addition, the algorithm of the program conservatively assumes the calculated deflections to remain constant when temperature gradients decrease (as occurs in the final

stages of fire tests on non-insulated walls). In STUD simulations, the values of Δ and y(z) at any given time step are not allowed to be less than in the previous step. This measure reflects the creep and stress relaxation phenomena in steel at temperatures higher than 400°C, and it was especially useful in lateral deflection simulations for Tests W4 and W6.

Simulated mid-height lateral deflection histories for Tests W1-W6 are presented in Figure 4 (lines with symbols). For these simulations, average temperatures measured at locations 2a and 4a in the central part of specimens, were used for T_H and T_C input, respectively. The value of $K_R = 0.6$ proved to produce a reasonably good agreement of simulated and measured deflections until the initiation of structural failure mechanisms in central studs. The structural failure of walls, however, doesn't occur for some time after that, due to the redistribution of load to colder studs at wall ends. The latter phenomenon is especially significant in insulated walls and in walls with wider stud spacing.

The major advantage of the proposed structural model is that it permits the simulation of both dominant failure modes, observed in tests, depending on the heating regime of the studs. As long as lateral deflections are properly simulated, the structural failure of studs can be predicted using conventional formulas from S136-94, for members subjected to combined compression and bending, adjusted to account for the deterioration of the mechanical properties of steel at elevated temperatures. The variation of steel yield strength with temperature can be evaluated using an expression by Gerlich et al. (1996)

$$F_{y\,T} = F_y \left(1.0 - 5.3 \cdot 10^{-4}\, T + 4.0 \cdot 10^{-6}\, T^2 - 1.9 \cdot 10^{-8}\, T^3 + 1.7 \cdot 10^{-11}\, T^4 \right) \qquad [13]$$

where $F_{y\,T}$ = steel yield strength at temperature T (in °C).

For insulated walls, the section near the stud end should be checked for the compressive failure of the hot flange. In STUD structural failure simulations for walls W1-W3 and W5, the perforated section at z = 0.2 H was checked, using the following failure criterion

$$f_H = n_H \left(\frac{P}{A^*_e} + \frac{P\,[e - y(0.2H)]}{S^*_{eH}} \right) \geq F_{yH} \qquad [14]$$

where
f_H = compressive stress at the extreme fibre of the hot flange,
n_H = reduction factor for temperature T_H, calculated using Eq.7,
$F_{y\,H}$ = yield strength of steel at temperature T_H, calculated using Eq.13,
A^*_e = elasticity-modulus-weighted effective stud section area in compression, and
S^*_{eH} = elasticity-modulus-weighted effective stud section modulus in bending that causes compression of hot flange.

Width of compression elements in effective stud cross-sections was reduced in accordance with Clause 5.6.2 of S136-94 to account for local buckling effects. For perforated sections, the web was considered to consist of two unstiffened elements, one on each side of perforation, according to Clause 6.8.1 of S136-94. Effective cross-section dimensions were assumed to be insensitive to temperature, thus, they were based on steel

properties at room temperature and compressive stress f = F_y. These effective cross-sections were used in the calculation of the temperature dependent 'modulus-weighted' properties A^*_e and S^*_{eH} (using an approach similar to evaluation of I* in Eq.8)

$$A^*_e = \sum_{i=1}^{q} n_i \, A_i \qquad [15]$$

$$S^*_{eH} = \sum_{i=1}^{q} n_i \, [I_i + A_i (x_i - c)^2] \Big/ (D - c) \qquad [16]$$

For non-insulated LSF walls, the section at (or near) stud mid-height should be checked for the compressive failure of the cold flange. In STUD structural failure simulations for walls W4 and W6, the perforated section at z = 0.4 H was checked, using the following failure criterion

$$f_C = n_C \left(\frac{P}{A^*_e} + \frac{P \, y(0.4H)}{S^*_{eC}} \right) \geq F_{yC} \qquad [17]$$

where
f_C = compressive stress at the extreme fibre of the cold flange,
n_C = reduction factor for temperature T_C , calculated using Eq.7,
F_{yC} = yield strength of steel at temperature T_C , calculated using Eq.13, and
S^*_{eC} = elasticity-modulus-weighted effective stud section modulus in bending that causes compression of cold flange, calculated from

$$S^*_{eC} = \sum_{i=1}^{q} n_i \, [I_i + A_i (x_i - c)^2] \Big/ c \qquad [18]$$

It should be emphasized that sectional properties A^*_e , S^*_{eH} and S^*_{eC} are based on three different effective cross-sections, because the configurations of compression elements are different in each case. Also note, that eccentricity, e, does not appear in Eq.17. As temperature gradients across the stud section decrease in the final stages of tests on non-insulated walls, the heating rate in cold flange becomes higher than in hot flange. This effect, combined with creep and stress relaxation phenomena in steel at temperatures higher than 400°C, causes gradual reduction of eccentricity. Therefore, the use of e = 0 in the expression for structural failure criterion is appropriate for non-insulated walls.

The STUD program conducts structural failure checks of Eqs. 14 and 17 at every time step in the simulation, thus, it can generate predictions of the structural failure time. Table 4 lists such predictions for Tests W1-W6 based on measured and TRACE-simulated temperatures. Predictions for non-insulated walls W4 and W6 show a reasonable agreement with test structural failure times. For insulated walls W1-W3 and W5, predicted failure times agree well with the initiation of structural failure in central studs. As expected, predictions based on measured temperatures generally show a better agreement with test results than predictions based on simulated temperatures.

Table 4. Comparison of predicted failure times with test results.

Assembly number	Insulation type (fibre)	Structural failure time in test (min.)	Initiation of failure in central studs in test (min.)	STUD predictions based on measured temperatures (min.)	STUD predictions based on simulated temperatures (min.)
W1	Glass	55	49	50	51
W2	Rock	73	50	52	52
W3	Cellulose	70	60	59	54
W4	-	76	N/A	77	73
W5	Rock	59	48	48	52
W6	-	83	N/A	84	85

SUMMARY

The behaviour of loadbearing LSF walls in standard fire resistance tests was discussed based on data from six experiments. Effects of loading, stud spacing, resilient channels and cavity insulation on fire resistance were analyzed. It was shown how stud loading conditions change during fire resistance tests. A comprehensive fire resistance model for loadbearing LSF walls was presented. Numerical techniques were demonstrated in heat transfer and structural simulations that produced a reasonable agreement with test results.

REFERENCES

Alfawakhiri, F. and Sultan, M.A. (1999) Fire Resistance of Load-Bearing Steel-Stud Walls Protected with Gypsum Board, *Proc. Fire and Materials '99*, Interscience Communications Ltd., San Antonio, TX, USA, 1:235-246.

ASTM E119-95a (1995) *Standard Test Methods for Fire Tests of Building Construction and Materials*, American Society for Testing and Materials, West Conshohocken, PA, USA.

CAN/ULC-S101-M89 (1989) *Standard Methods of Fire Endurance Tests of Building Construction and Materials*, Underwriters' Laboratories of Canada, Scarborough, ON, Canada.

Gerlich, J.T., Collier, P.C.R. and Buchanan, A.H. (1996) Design of Light Steel-Framed Walls for Fire Resistance, *Fire and Materials*, 20(2): 79-96.

Kodur, V.K.R., Sultan, M.A. and Alfawakhiri, F. (1999) Fire Resistance Tests on Loadbearing Steel Stud Walls, *Proc. 3rd International Conference on Fire Research and Engineering*, Society of Fire Protection Engineers, Chicago, IL, USA, 1:275-286.

Lie, T.T. (1992) *Structural Fire Protection*, American Society of Civil Engineers, New York, NY, USA.

NBCC (1995) *National Building Code of Canada*, Canadian Commission on Building and Fire Codes, National Research Council of Canada, Ottawa, ON, Canada.

S136-94 (1994) *Cold Formed Steel Structural Members*, Canadian Standards Association, Etobicoke, ON, Canada.

Sultan, M.A. (1996) A Model for Predicting Heat Transfer Through Non-insulated Unloaded Steel-Stud Gypsum Board Wall Assemblies Exposed to Fire, *Fire Technology*, 32: 239-259.